A 3D Numerical Method for Studying Vortex Formation Behind a Moving Plate

T. Y. Hou[1,*], V. G. Stredie[1] and T. Y. Wu[2]

[1] *Department of Applied and Computational Mathematics, California Institute of Technology, Pasadena, CA 91125, USA.*
[2] *Department of Mechanical Engineering, California Institute of Technology, Pasadena, CA 91125, USA.*

Abstract. In this paper, we introduce a three-dimensional numerical method for computing the wake behind a flat plate advancing perpendicular to the flow. Our numerical method is inspired by the panel method of J. Katz and A. Plotkin [J. Katz and A. Plotkin, Low-speed Aerodynamics, 2001] and the 2D vortex blob method of Krasny [R. Krasny, *Lectures in Appl. Math.*, 28 (1991), pp. 385–402]. The accuracy of the method will be demonstrated by comparing the 3D computation at the center section of a very high aspect ratio plate with the corresponding two-dimensional computation. Furthermore, we compare the numerical results obtained by our 3D numerical method with the corresponding experimental results obtained recently by Ringuette [M. J. Ringuette, Ph.D. Thesis, 2004] in the towing tank. Our numerical results are shown to be in excellent agreement with the experimental results up to the so-called formation time.

Key words: Aerodynamics; vortex dynamics; potential flows.

1   Introduction

This work is inspired by our desire to develop a 3D computational method to study the fluid dynamics of flying animals like birds or fish. Flight has fascinated the human mind since its early days of development. The gracefulness and the perfection of a bird in the air inspired us to try to emulate some particular aspects of its superb ability. The fluid dynamics in the flight of a bird is extremely complex and interesting. In particular, we are interested in understanding the way that the wake is generated and its effect on the wing. A number of computational methods have been developed to study fluid dynamics of the motion of a moving surface. However, it is

---

*Correspondence to: T.Y. Hou, Department of Applied and Computational Mathematics, California Institute of Technology, Pasadena, CA 91125, USA. Email: `hou@acm.caltech.edu`

still a challenge to develop an accurate and efficient three dimensional computational method which can be used to simulate the flight of a bird.

There have been many theoretical and computational studies to understand the fluid dynamics instability for flow past a flexible object. Starting with the work of Sir James Gray who was the head of Cambridge University's Zoology Department from 1937 to 1961, the theory of animal locomotion stimulated G. I. Taylor in making two pioneering investigations. One involved the swimming of snakes and eels, and the other one initiated hydrodynamic studies of flagellar propulsion. However, the main contributions to this domain came later on from Sir James Lighthill and Professor Theodore Wu. Lighthill laid a theoretical foundation for the swimming of slender fish, while Wu made an extension of classical oscillating airfoil aerodynamics to a linear theory of flexible lifting-surface locomotion, to examine the performance of bending wings of birds in flapping flight and the lunate tails of fast-swimming percomorph and acombroid fishes and rays in swimming.

Re-emphasizing the importance of Wu's (scaling of aquatic locomotion- [21]), Lighthill's (scaling of aerial locomotion) and Weis-Fogh's (hovering flight) work in fish and bird locomotion, we should also review the advances made in the field of wing theory and free-surface numerical methods. One of the pioneers in the study of a wing in flight was T. Theodorsen with his theory of instability and the mechanism of flutter [18]. In 1931, Kaden introduced similarity variables for describing the roll-up of a semi-infinite plane vortex-sheet ([17], p. 147). During the 1950s, several authors presented approximate asymptotic solutions in which the spiral vortex generated behind a sharp edge was replaced by a single point vortex, an example of which was given by [16]. Moore in 1976 [12] studied and verified the stability of a class of vortex sheets roll-up, but could not verify the stability of the problem as noted by Pullin in 1978 [14]. In the same work of Pullin, he obtained for the first time regular and well-defined start-up vortex spirals from an accurate numerical solution of the Birkhoff-Rott equation (inviscid flow) written in similarity variables. These results were later used by Krasny to validate his method.

In 1991, Krasny [10] generalized Chorin's vortex blob method [3] and applied it to study the evolution of the wake forming at the edges of a flat plate advancing perpendicular to the flow. Moreover, he presented strong numerical evidence suggesting that the vortex blob method converges past the vortex sheet singularity formation time, as the smoothing parameter tends to zero. Later on, in 1994, Nitsche and Krasny [13] generalized the vortex blob method to study the vortex ring formation at the edge of a circular tube. Comparison between the numerical simulation and the corresponding experiment indicated that the model captured the basic features of the ring formation process. Then, in 2001, a very interesting model was presented by Chamara and Coller [2] for a pair of airfoils with two degrees of freedom: pitching and heaving. Their study sheds interesting light in finding the optimal configuration of the two-airfoil system for which the two oscillatory instabilities due to the flutter occur simultaneously.

In the study of animal locomotion, Dickinson *et al.* designed interesting experiments to measure the unsteady forces on a robotic fruit fly wing and demonstrated the role of wing rotation in force generation [6]. In a related effort, Wang in 2000 [20] tried to quantify the vortex dynamics of a flying insect and identified a minimal two-dimensional model that produces sufficient lift. Later, in 2004, Wang, Birch and Dickinson [19] compared computational, experimental and

quasi-steady forces in a generic hovering wing undergoing sinusoidal motion along a horizontal stroke plane. In particular, they investigated unsteady effects and compared two-dimensional computations and three-dimensional experiments in several qualitatively different kinematic patterns.

In three dimensions we should point to the work of Brady, Leonard and Pullin in 1998 [1] who provided a three-dimensional computational method to track the evolution of regularized three-dimensional vortex sheets through an irrotational, inviscid, constant-density fluid. Also, in 2001, Lindsay and Krasny [11] developed a fast adaptive Lagrangian particle method for computing free vortex sheet motion in three dimensional flow. To be able to do all the computations efficiently, they also included an adaptive treecode algorithm.

In this paper we propose a three-dimensional numerical method for a flat plate advancing perpendicular to the flow. The three-dimensional approach for the computation of the bound circulation is inspired from the panel method presented in "Low speed aerodynamics" by J. Katz and A. Plotkin [9]. This is combined with Krasny's two-dimensional method to solve for the free sheet vortex elements. The accuracy of the method will be demonstrated by comparing the 3D computation at the center section of a very high aspect ratio plate with the corresponding two-dimensional computation. For a high aspect ratio plate, the three dimensional effect at the center section of the plate is very small. We found excellent agreement between our 3D computations and the corresponding 2D ones. We also perform careful computations to compare our results with a recent physical experiment by Ringuette at Caltech involving a three-dimensional flat plate advancing perpendicular to the flow [15]. Our numerical results match very well the experiments by Ringuette in terms of the total circulation along chord-wise sections of the wake until the so-called formation time. After the formation time, Ringuette observed that vortex separation occurred and circulation grew slower than the circulation obtained by our numerical method. This discrepancy could be due to the viscous effect which cannot be modeled accurately by our inviscid model based in potential flow theory.

The three-dimensional results are important for developing a more complex three dimensional theory. This could be the first step toward a more in-depth analysis. Currently, our 3D numerical method still does not capture accurately the true 3D effect near the corners of the plate due to our simplified approximation of the circulation along the longitudinal and transversal sections by a two-dimensional model. In our future work, we plan to develop a more accurate 3D theory that captures the essential 3D nonlinear effects. One way to achieve this is to generalize a recent theory of Wu [22] to three space dimensions. In Wu's theory, strong nonlinear effect of the flow is captured analytically. This provides very accurate approximation to the amount of vorticity shed at the trailing edge of the plate, which has leading order effect on the overall accuracy of the computation. We have already performed very thorough computational study of Wu's method in [8] for various severe tests. We found that the numerical method based on Wu's theory can capture accurately the leading singular effect near the trailing edge, which improves the accuracy when dealing with some highly nonlinear movements. Generalization of Wu's theory to three dimensions is a challenging task. The results obtained in this paper can provide the basis for our future study along this direction.

The rest of the paper is organized as follows. In Section 2, we will review Krasny's vortex blob

method for the two dimensional case and present a numerical experiment for a wing advancing upward, normal to the flow. In Section 3, we will present our three-dimensional computational method. We will test our 3D numerical method for a high aspect ratio plate and compare our results with those obtained by the two-dimensional vortex blob method. We will also perform some very interesting comparison with the experiments obtained by Ringuette [15]. Section 4 is devoted to some concluding remarks.

2 Vortex formation at the edges of a free falling 2D plate

In this section, we will review Krasny's two dimensional vortex blob method which is used to compute fluid motion of a flat plate advancing normal to the flow. In this case, the flow generates a vortex sheet roll-up at the edges of the plate. In the next section, we will show how to generalize Krasny's method to three space dimensions by borrowing ideas from the panel method of J. Katz and A. Plotkin [9]. The two dimensional method presented in this section will be later used to check the accuracy of our three dimensional method for a very high aspect ratio plate.

2.1 Description of the 2D vortex blob method

In two space dimensions, we can define a vortex sheet by a curve $z(\Gamma, t)$ in the complex plane, where Γ is circulation. The velocity distribution along the vortex sheet will be chosen as the average of the velocity distributions above and below the vortex sheet. Using the Biot-Savart law, one can derive an evolution equation for the vortex sheet as follows (as known as the Birkhoff-Rott equation)

$$\overline{\frac{\partial z}{\partial t}}(\Gamma, t) = \int K(z(\Gamma, t) - z(\tilde{\Gamma}, t)) d\tilde{\Gamma}, \qquad K(z) = \frac{1}{2\pi \imath z}, \tag{2.1}$$

where the Cauchy principal value of the integral is taken, and $\bar{z}$ stands for the complex conjugate. The Biot-Savart kernel $K(z)$ has a simple pole singularity at $z = 0$. In the vortex blob method, the singular kernel K in (2.1) is replaced by a regularized one, K_δ, with δ being a small smoothing parameter. As δ approaches to zero, $K_\delta(z)$ approximates $K(z)$ for $z \neq 0$. For the two-dimensional vortex sheet problem, Krasny [10] uses the following regularization for K_δ:

$$K_\delta(z) = K(z) \frac{|z|^2}{|z|^2 + \delta^2}. \tag{2.2}$$

With such regularization, the integral equation fro $z(\Gamma, t)$ is no longer singular.

We will use the trapezoidal rule to approximate the velocity integral. Let Γ be parameterized by a Lagrangian variable α. Therefore, the interface position $z(\Gamma, t)$ is a function of α as well. We discretize α by a uniform grid with mesh size h, and denote $\alpha_j = jh$ with j being integer. Further, we denote $\Gamma_j = \Gamma_\alpha(\alpha_j)h$, and $z(\Gamma(\alpha_j), t) = z_j(t)$. With these notations, the integral

equation can be discretized by the trapezoidal rule as follows:

$$\overline{\frac{\partial z_j}{\partial t}} = \sum_k K_\delta(z_j - z_k)\Gamma_k. \tag{2.3}$$

Furthermore, by discretizing in time using a 4th order Runge-Kutta method or a multi-step method, one can obtain a fully discrete system for the evolution of $z_j(t)$.

In Krasny's method [10], the plate coincides with the interval $-1 \leqslant x \leqslant 1$ and it moves vertically with speed $1/2$. The flow contains a bound vortex sheet, which is discretized with point vortices, and a free vortex sheet, which is discretized with vortex blobs. At every time step, a new filament is released from both edges of the plate. It follows from equation (2.3), the velocity at a vortex element centered at (x_j, y_j) is given by

$$(\frac{dx_j}{dt}, \frac{dy_j}{dt}) = \sum_{k \neq j} \frac{(-(y_j - y_k), (x_j - x_k))\Gamma_k}{2\pi((x_j - x_k)^2 + (y_j - y_k)^2 + \delta^2)}. \tag{2.4}$$

We remark that δ is set to zero whenever the index k refers to one of the bound point vortices. Along the bound sheet, since the plate is horizontal, i.e., y is constant, the bound vortex sheet strength $\gamma(x, t)$ satisfies a Cauchy singular integral equation of the first kind,

$$\frac{1}{2\pi} \int_{-1}^{1} \frac{\gamma(\tilde{x}, t)d\tilde{x}}{(x - \tilde{x})} = v(x, t). \tag{2.5}$$

The reason for using point vortices on the bound sheet is because the resulting linear system for a general right side may not be invertible if the kernel is smoothed, as Krasny pointed out. To provide better resolution at the edges, the bound point vortices are not placed uniformly on the plate, instead they cluster toward the edges according to $x_j = \cos\theta_j, \theta_j = j\pi/n$ and equation (2.5) is satisfied at the midpoint of each interval. To close the system, we need another equation. To find this extra equation, we use the fact that the total circulation is conserved in accordance with Kelvin's theorem. When supplemented with this additional equation, equations (2.5) transform into a linear system which is invertible. Upon solving this linear system, we obtain the strengths $\gamma(x_j, t)$.

Now it comes to the important question: how to generate the first released free vortice from the edge of the plate. To do this, one needs to take into account the viscous effect. Krasny uses the Kutta condition to determine the circulation of the first released free vortice near the edge of the plate:

$$\frac{d\Gamma}{dt} = \frac{1}{2}(U_-^2 - U_+^2) = \overline{U} \cdot \gamma, \tag{2.6}$$

where $\gamma \sim \Delta\Gamma/\Delta x$ is calculated by a finite difference formula. Here, U_- and U_+ are the one-sided velocities at the edge, $\overline{U}$ is the average velocity, and γ is the vortex sheet strength at the edge. The slip velocities satisfy

$$U_- - U_+ = \gamma, \qquad \frac{1}{2}(U_+ + U_-) = \overline{U}. \tag{2.7}$$

Further, we need to enforce a separating flow condition to prevent an attached slip flow from contributing to the shedding process. This condition is enforced by setting $U_+ = 0$ if $U_+ < 0$ and similarly setting $U_- = 0$ if $U_- < 0$. Krasny's method also uses an adaptive point insertion technique and an adaptive time step to provide adequate numerical resolution.

Krasny performed numerical experiments to compare his results with the ones obtained by Pullin in 1978. Pullin used point vortices to represent the vortex sheet with a single point vortex to represent the inner spiral turns. Moreover, Pullin used conformal mappings to determine the strength of the bound vortex sheet. Krasny found that the pair of counter-rotating vortices forming in the recirculating region behind the plate agree very well between the two methods.

2.2   A numerical example

In this subsection, we present a numerical example using Krasny's vortex blob method to model the wake behind a two-dimensional plate advancing perpendicular to the flow. More details can be found in [10].

The implementation of Krasny's method consists of the following steps: (i) form a linear system for the circulation at the discrete vortices, (ii) solve the linear system to obtain the circulation, (iii) determine the velocity of the currently released free filament. The system will be formed based on the evolution equation (2.1) with a smoothed kernel given by (2.2). The discretization of this equation is given by (2.4). The unkowns of the linear system are the circulation of the bound point vortices. Since the problem is symmetric we have a stationary point in the center of the plate with zero circulation.

In our implementation we take $N + 1 = 81$ points on a plate with radius $R = 1$ which moves upward with a velocity $U_0 = 1/2$. The plate reaches this velocity after an acceleration that takes $t = 0.01$. During this acceleration the time-steps are smaller than $dt = 0.01$ but they increase linearly. When the velocity becomes constant (at $U_0 = 1/2$), the time step becomes constant as well, with $dt = 0.01$. We choose this approach to make the transition from velocity zero to the steady state velocity smoother. In the computation, the blob is chosen to be $\delta = 0.2$ and the grid points for the bound vortex distribution along the wing have a cosine distribution so that we have more points and therefore a better resolution at the edges of the plate. The boundary condition requires that there be no normal flow through the plate. This means that we need to match the normal velocity from (2.4) with the advancing velocity of the plate. This will be done at the midpoint of each subinterval $[z_j, z_{j+1}]$, which gives N equations. However we need to compute the circulation at every bound point, which has a total of $N + 1$ unknowns. We need one more equation. This extra equation can be obtained by the fact that we have a stationary point in the center of the plate with zero circulation. Hence, we have a linear system with $N + 1$ equations and $N + 1$ unknowns which will be solved by inverting the matrix in Matlab with the *inv* function. This provides the circulation on the plate.

The sheet strength value at the edge of the plate γ_e, will be computed by a finite difference formula applied to the bound circulation $\gamma \sim \Delta\Gamma/\Delta x$. The edge strength will allow us to compute the circulation and the velocity of the newly shed vortex. For that we will use (2.6). First, we compute the averaged slip velocities $\overline{U}$ at both edges of the plate. This will be done
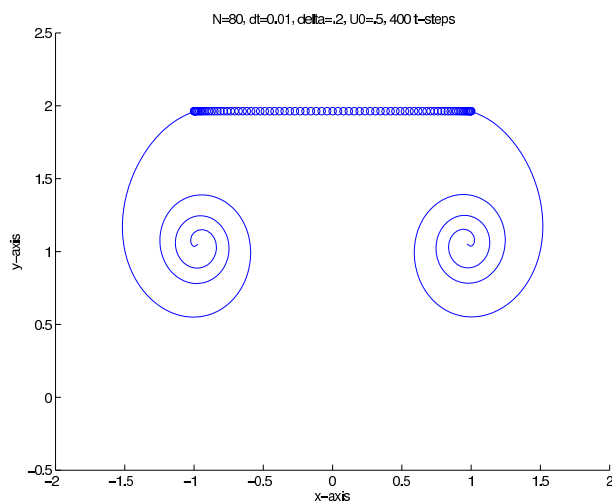
Figure 1: Krasny's method for a wing advancing upward, normal to the flow, with adaptive speed $U_0 \approx 0.5$, blob $\delta = 0.2$, variable time-step $dt \approx 0.01$. Plot after 400 time steps having $N = 80$ bound vortex points.

using relation (2.4). Then we compute the slip velocities above and below the edge U_+ and U_- using (2.7). If either U_+ or U_- is negative, we set it to zero to prevent attached slip flow. With the updated U_+ and U_- we recompute $\overline{U}$, which will be now the tangential velocity of the currently released vortex filament, and compute the circulation of this free filament from (2.6).

Remark 2.1. In (2.6), $d\Gamma/dt$ represents the time variation of the total circulation of the free sheet. Moreover, the newly shed vortex filament is released tangentially to the plate, i.e. in the x-direction, with the computed tangential velocity $\overline{U}$.

The numerical computation for Fig. 1 is performed with the data described above and a blob size $\delta = 0.2$. The plot is obtained after 400 time-steps. We can see a very nice roll-up which agrees very well with the results obtained by Krasny [10] and Pullin [14].

3   Three-dimensional model

In this section, we will present a three-dimensional computational method to study the vortex motion behind a wing advancing upward. Our three dimensional model is motivated by a panel-method and Krasny's vortex-blob method for two space dimensions. We will first describe our 3D method for a square flat plate. Later on, we will apply our 3D method to a rectangular plate with very high-aspect ratio. In this case, the three dimensional effect is relatively small near the center section of the plate. We then compare the numerical results obtained by our 3D method with those obtained by the corresponding 2D method and find very good agreement. We also

compare our numerical results with some recently performed physical experiment in a towing tank. The agreements are excellent before the formation time.

We now describe our 3D numerical method. First, we would like to form a linear system using the Biot-Savart law by imposing the normal flow conditions on the plate, and to determine the circulation of the plate filaments by solving this system. We apply a rectangular mesh over the plate and use more mesh points near the corners and edges to give a better resolution. The mesh will form some panels on the wing and we will apply the no-through flow condition in the center of each one. After computing the bound circulation for the panels, we will compute the circulation for each filament on the plate, and then apply the two-dimensional method along all the longitudinal and transversal sections. The two-dimensional method will be used to compute the circulation of the currently shed vortex filament. Note that the filament is shed at every time step along the mesh lines. The circulation of all the other free filaments will be preserved in time. Thus we have all the quantities to compute the velocities of all the free filaments. We then move these filaments to the updated locations and go to the next time step. We will describe the algorithm in some details in the next subsection.

We should point out that the above procedure does not capture all the three dimensional effect of the Euler equations. By using a two-dimensional method to compute the circulation along all the longitudinal and transversal sections, we make certain approximation of the 3D Euler equations. The approximation is relatively poor near the corners of the plate. On the other hand, certain essential 3D effect is captured by our model using the panel method to be described below. As you will see in our numerical experiments, our 3D numerical method gives a reasonably good approximation to the fully 3D physical experiments for a plate advancing upward to the flow, despite the approximation we make in the model.

3.1   Velocity for the bound sheet

Next we will compute the velocity field induced by each vortex panel. It is known that the velocity induced by a vortex filament of strength Γ and a length of dl is given by the law of Biot and Savart

$$d\vec{V} = \frac{\Gamma(\vec{dl} \times \vec{r})}{4\pi r^3}. \tag{3.1}$$

From Fig. 2 the magnitude of the induced velocity is

$$dV = \frac{\Gamma \sin \theta dl}{4\pi r^2}. \tag{3.2}$$

Since we are interested in the flow field induced by a straight segment, let us use the above equations to calculate this effect. Let AB be such a segment, with the vorticity vector directed from A to B. Let C be a point in space whose normal distance to line AB is r_p. Since

$$r = \frac{r_p}{\sin \theta} \qquad \text{and} \qquad dl = r_p(\csc^2 \theta)d\theta, \tag{3.3}$$

we can integrate between A and B to find the magnitude of the induced velocity

$$V = \frac{\Gamma}{4\pi r_p} \int_{\theta_1}^{\theta_2} \sin \theta d\theta = \frac{\Gamma}{4\pi r_p}(\cos \theta_1 - \cos \theta_2). \tag{3.4}$$
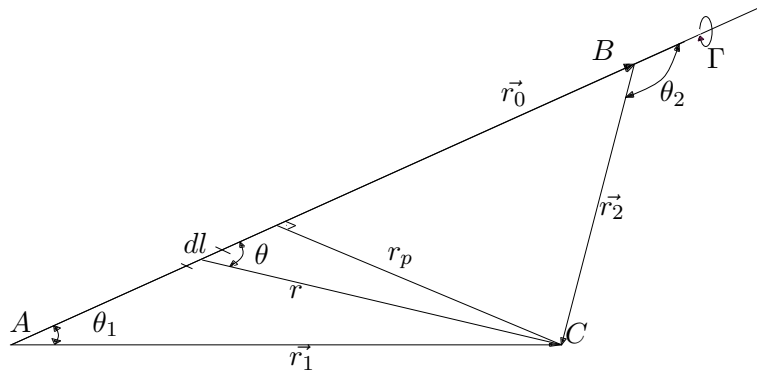
Figure 2: Velocity induced by vortex segment $\vec{AB}$ at location C.

Now let $\vec{r_0}, \vec{r_1}$ and $\vec{r_2}$ designate the vectors $\vec{AB}, \vec{AC}$ and $\vec{BC}$, respectively, as shown in Fig. 2. Then we have

$$r_p = \frac{|\vec{r_1} \times \vec{r_2}|}{r_0}, \quad \cos\theta_1 = \frac{\vec{r_0} \cdot \vec{r_1}}{r_0 r_1}, \quad \cos\theta_2 = \frac{\vec{r_0} \cdot \vec{r_2}}{r_0 r_2},$$

where for a vector $\vec{r}$, we denote by r its magnitude. Substituting these expressions into equation (3.4) and noting that the direction of the induced velocity is given by the unit vector

$$\frac{\vec{r_1} \times \vec{r_2}}{|\vec{r_1} \times \vec{r_2}|},$$

we get

$$\vec{V} = \frac{\Gamma}{4\pi} \frac{\vec{r_1} \times \vec{r_2}}{|\vec{r_1} \times \vec{r_2}|^2} \left[\vec{r_0} \cdot \left(\frac{\vec{r_1}}{r_1} - \frac{\vec{r_2}}{r_2} \right) \right]. \tag{3.5}$$

Now in order to implement this, we write the components of the induced velocity $V = (u, v, w)$

$$\begin{cases} u = K \cdot (r_1 \times r_2)_x \\ v = K \cdot (r_1 \times r_2)_y \\ w = K \cdot (r_1 \times r_2)_z \end{cases}, \qquad K = \frac{\Gamma}{4\pi |r_1 \times r_2|^2} \left(\frac{r_0 \cdot r_1}{r_1} - \frac{r_0 \cdot r_2}{r_2} \right) \tag{3.6}$$

where

$$\begin{cases} r_0 \cdot r_1 = (x_2 - x_1)(x_p - x_1) + (y_2 - y_1)(y_p - y_1) + (z_2 - z_1)(z_p - z_1), \\ r_0 \cdot r_2 = (x_2 - x_1)(x_p - x_2) + (y_2 - y_1)(y_p - y_2) + (z_2 - z_1)(z_p - z_2), \end{cases} \tag{3.7}$$

and $|r_1 \times r_2|^2 = (r_1 \times r_2)_x^2 + (r_1 \times r_2)_y^2 + (r_1 \times r_2)_z^2,$

$$\begin{cases} r_1 = \sqrt{(x_p - x_1)^2 + (y_p - y_1)^2 + (z_p - z_1)^2}, \\ r_2 = \sqrt{(x_p - x_2)^2 + (y_p - y_2)^2 + (z_p - z_2)^2}, \end{cases} \tag{3.8}$$
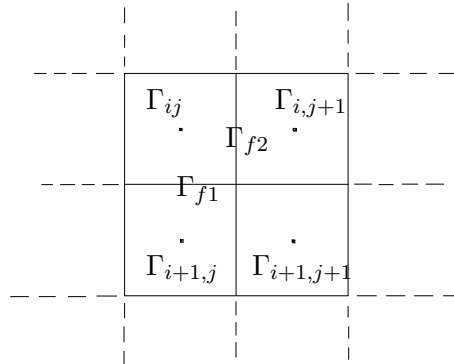
Figure 3: Computing the filament circulations from the panel circulations.

and

$$\begin{cases} (r_1 \times r_2)_x = (y_p - y_1)(z_p - z_2) - (z_p - z_1)(y_p - y_2), \\ (r_1 \times r_2)_y = -(x_p - x_1)(z_p - z_2) + (z_p - z_1)(x_p - x_2), \\ (r_1 \times r_2)_z = (x_p - x_1)(y_p - y_2) - (y_p - y_1)(x_p - x_2). \end{cases} \qquad (3.9)$$

We will consider a 2 by 2 square plate and a N by N grid on top of it, with N odd so that a vortex point will be placed in the center of the plate. By imposing the no-through flow conditions in the center of the mesh panels we will get $(N-1)^2$ linear equations using formula (3.5). To each panel we assign a circulation $\Gamma_{i,j}$, meaning that all filaments bordering that panel will have the same circulation $\Gamma_{i,j}$. At time $t = 0^+$, before anything is shed into the free sheet, the linear system will look like this

$$\begin{aligned} & a_{11}\Gamma_{1,1} + a_{12}\Gamma_{1,2} + a_{13}\Gamma_{1,3} + \ ... \ + a_{1,(N-1)^2}\Gamma_{(N-1),(N-1)} = U_0 \\ & a_{21}\Gamma_{1,1} + a_{22}\Gamma_{1,2} + a_{23}\Gamma_{1,3} + \ ... \ + a_{2,(N-1)^2}\Gamma_{(N-1),(N-1)} = U_0 \\ & ... \\ & a_{(N-1)^2,1}\Gamma_{1,1} + a_{(N-1)^2,2}\Gamma_{1,2} + \ ... \ + a_{(N-1)^2,(N-1)^2}\Gamma_{(N-1),(N-1)} = U_0, \end{aligned} \qquad (3.10)$$

where the left hand side of each equation represents the sum of the velocities induced on a given panel by the $(n-1)^2$ panel circulations. Whenever we compute the velocity induced by a panel on a certain point (center of panels), we implicitly consider the contribution from each segment filament bordering the panel so that every such segment will give two contributions. One segment filament will enter the calculations from both panels it belongs to, having opposite oriented circulations in the two panels. Hence, in our 3D numerical method, the circulation of each filament is the difference of the circulations of the panels that the filament borders. Specially, after solving the linear system for the circulation of each panel, we will compute the circulation of each filament as the difference of circulations of the panels which have the filament

as a common interface, see Fig. 3. We get

$$\Gamma_{f1} = \Gamma_{i,j+1} - \Gamma_{ij}, \quad \text{and} \quad \Gamma_{f2} = \Gamma_{i+1,j} - \Gamma_{ij}. \tag{3.11}$$

Note that the velocity induced by a filament is taken into consideration two times, one time for every panel it belongs to. These filament circulations are the ones that we will be using in the next subsection to analyze the two dimensional flow along each longitudinal and transversal plate section.

3.2   Velocity for the free sheet

We found a very simple and elegant way to solve for the free sheet. At this point we know how to solve for all the quantities on the bound sheet. We also know the circulation along all the chord-wise and span-wise sections. From now on, we will switch to the two-dimensional method and apply it for all these sections with the given steady-state bound circulation, imported from the three-dimensional model. As in Section 2.2, we will compute for every such two-dimensional slice the sheet strength value at the edge γ_e, which will give us the slip velocities $\overline{U}$ at both edges. Furthermore, we will compute the slip velocities above and below the edge and impose the non-attached slip flow condition. With the updated slip velocities we will recompute $\overline{U}$, which is now the velocity of the currently released vortex filament, and recompute the circulation of this free vortex from (2.6).

   Having all the information about the first free vortex element we can now move it according to $\overline{U}$. Going to the next time step, we will solve the corresponding section's two-dimensional linear system. However, from now on the contributions from the previously released free vortices will enter the system. Their circulation will be known since it is preserved in time, and therefore, as discussed in Subsection 2.1, we can write the system as

$$A\tilde{\Gamma} = \tilde{b}, \tag{3.12}$$

where A is the matrix of coefficients from the two-dimensional model, $\tilde{\Gamma}$ is the new bound circulation to be computed, and $\tilde{b}$ is the known vector, including the circulation induced by the free vortex elements. We can look at this system as a perturbed system from its original state. Consider $\tilde{b} = b + \delta b$, where b is the vector from time step one consisting only of the imposed normal velocities. We add to this normal velocity some perturbation δb which is in fact the velocity induced by the free vortices. Then, we can also write $\tilde{\Gamma} = \Gamma + \delta\Gamma$, where Γ is the wake-less bound circulation imported from the three-dimensional model. Hence we get

$$A(\Gamma + \delta\Gamma) = b + \delta b. \tag{3.13}$$

But A, Γ and b solve the initial linear system at time $t = 0$ so $A\Gamma = b$ and therefore (3.13) becomes

$$A \cdot \delta\Gamma = \delta b. \tag{3.14}$$

Solving this system we get $\delta\Gamma$ and hence the new bound circulation $\Gamma + \delta\Gamma$. All the other quantities: the edge strength, the slip velocities and the velocities of the free vortices, are computed at every time step from the two-dimensional model, using the known bound circulation.
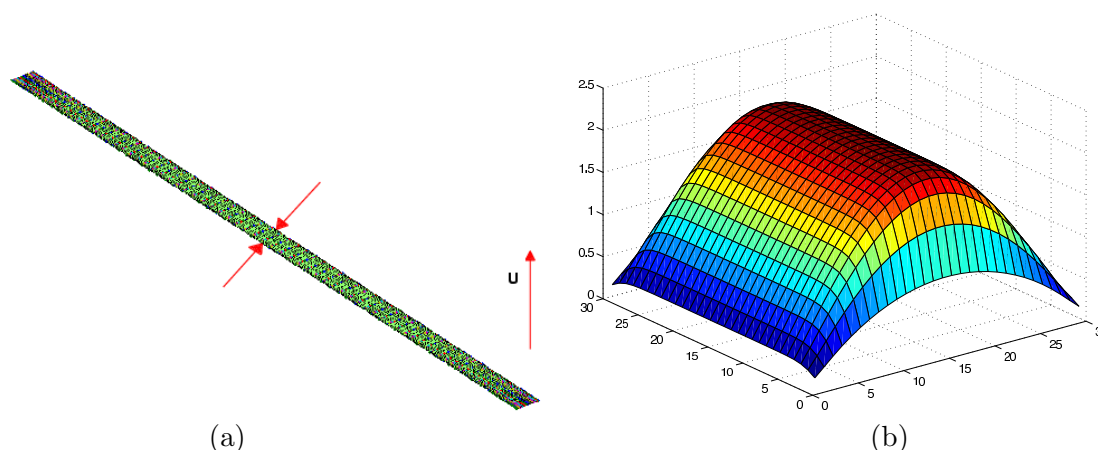
Figure 4: (a) three-dimensional high aspect ratio wing and section being considered; (b) Plot of steady-state circulation as given by Eq. (3.5).

3.3   A 3D computation for a very high aspect ratio plate

To check the accuracy of our three-dimensional method, we apply our 3D numerical method for a very high aspect ratio plate, and compare our results with the corresponding computations obtained by the two-dimensional method. For a very high aspect-ratio plate, the three-dimensional effect in the center section should be very small. We expect the center section to behave very similar to the two-dimensional plate we studied in Section 2.2. We analyze a three-dimensional plate of length 62 and width 2. The mesh consists of 31x31 points and they are placed according to some cosine distribution so that we have more points in the corners and therefore better accuracy. We will compare the steady-state circulation (no wake influence) of the center section of this plate with the two-dimensional model which has a length of 2 and a mesh of 31 points as well. The wings will advance upward with a speed $U = 1$.

Fig. 4(a) shows the wing and the section we are considering and Fig. 4(b) shows what the steady-state panel circulation looks like on the wing. To get similar results to the two-dimensional case we have to use Eq. (3.11) and compute the circulation of the filaments on the section being considered. Plotting this on top of the two-dimensional circulation (see Fig. 5(a)) we get results so close they are almost indistinguishable. The norm of their difference is very small, around $2.4842 \cdot 10^{-4}$. This difference is still larger than the computer precision, showing the presence of the three-dimensional effect.

Fig. 5(b) shows the circulation in the section which is closest to the edge of the wing in a chord-wise section. We can notice that even though the shape looks similar, the absolute value of the circulation of the filaments is lower than in the center section, being about half of the latter. Fig. 5(c) shows the circulation along the center section in a span-wise plane, and this is quite different than the other two. The circulation being very small for the main part of this section shows that the edge effects become very small as we go further from the plate's edges. In fact it says that only about 22% of the plate near every edge will feel the finite-wing effect. The
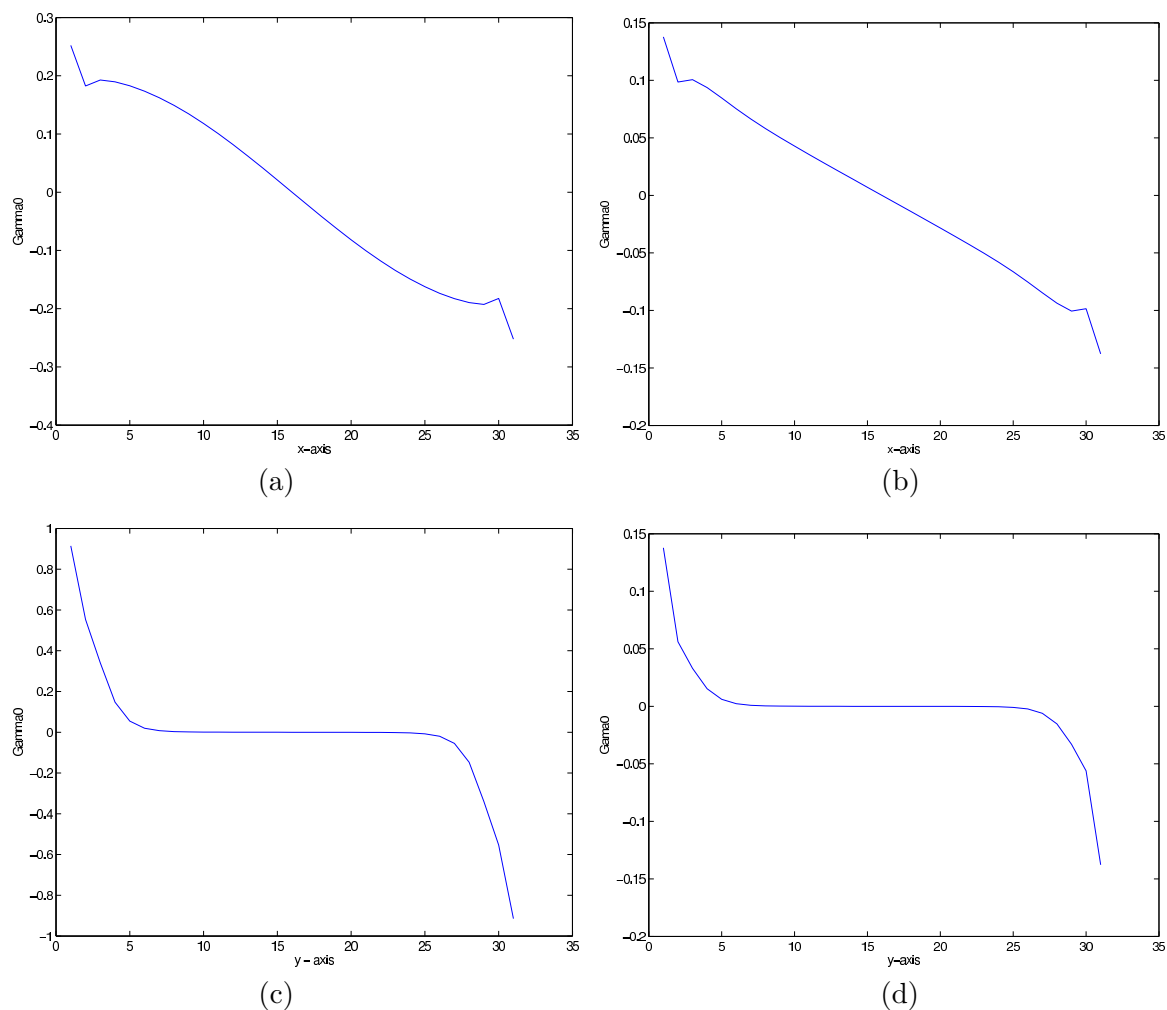
Figure 5: (a)&(b) chord-wise sections; (c)&(d) span-wise sections; (a) Superposition of circulation obtained in the two-dimensional case and the one obtained in the three-dimensional center chord-wise section; (b) Circulation obtained in the three-dimensional case, on an edge chord-wise section; (c) Circulation for the three-dimensional case on the central span-wise section; (d) Circulation for the three-dimensional case on an edge span-wise section.

last plot, Fig. 5(d), gives the circulation on the plate for a section near the edge in a span-wise plane. Note that this is significantly smaller than the circulation for the corresponding center section, being about 6 times smaller. In conclusion, our model proves to be very accurate when compared with the two-dimensional one. Figs. 5(b), 5(c) and 5(d) show how important the three-dimensional effect is in the motion of the plate, especially at the edges. They also show that the finite-plate effect tends to reduce the vorticity in the near-edge cross sections compared to the center ones.

3.4   Numerical results vs. experiment for a rectangular wing

In this section we compare our 3D numerical method with physical experiments performed in a towing tank. Before we present the comparison of our numerical results with the experimental results, we consider some wings with aspect ratios (AR) found in various birds and insects. Aspect ratio here will be defined as b^2/S, where b is the span of a single wing, instead of the conventional definition, which is the distance between both wing tips; S is the single-wing planform (top-view) area. Flying insects have AR's between about 2.75 and almost 6 [6, 7] while hummingbirds have AR's of around 4 [5]; a soaring bird, such as albatross, has an AR of about 9 [5]. A finite aspect-ratio wing, compared to one of infinite span, experiences aerodynamic effects due to the tip, which increase relatively as the aspect ratio decreases. Therefore for low aspect ratio wings the influence of the tip is very significant.

In this subsection, we compare our numerical results obtained by solving our 3D numerical method with the experiments performed by Ringuette [15] in the GALCIT towing tank at California Institute of Technology. Given the aspect ratios found in insects and hummingbirds mentioned above, he made some experiments with flat plates of rectangular platforms, having $AR = 2$ and $AR = 6$. Next, we will compare these experiments with the result obtained with our numerical method.

One thing the reader should be aware of is the presence of vortex separation in Ringuette's work. He argues that the circulation of the vortex ring does not grow indefinitely. Therefore, the experiments will show separation which happens at a time called "formation number". Formation number is the non-dimensional time at which a vortex achieves its maximum circulation before pinch-off. Pinch-off occurs when a vortex is no longer being fed by the shear-layer that generated it and the two become distinct entities in terms of vorticity. This separation was found in the experiment, however we can not observe this from our numerical experiment. Of course, if we wanted to mimic the experiment even better we could artificially detach the leading edge vortex (LEV) in our numerical method and let another one begin forming.

Aspect Ratio 2

For a wing of aspect ratio 2, the effects due to the tip are more prevalent than the case with $AR = 6$. It can be seen from Fig. 6 that the vortices near both chord-wise and span-wise center sections have more roll-ups than the ones near the corresponding edges. This is in perfect agreement with what we found in the previous subsection, where we showed (see Fig. 5) that there is more circulation near the bound center sections than near the edges. This will imply that less circulation is shed in the free sheet near the edges, making the vortices weaker. Also from the same plots (see Fig. 5) we expect the vortices to be stronger along the chord wise sections compared to those released along span-wise sections since the corresponding total circulation is bigger.

In both numerical and experimental setup a plate with chord $c = 5$ and aspect ratio $AR = 2$ is used (for the experiment the measuring unit was centimeter). The plate velocity is $U_0 = 6$ and for the numerical method we choose a time step of $dt = 0.003$ and a blob $\delta = 0.2$. Our numerical bound sheet is represented by a 31x31 point mesh.
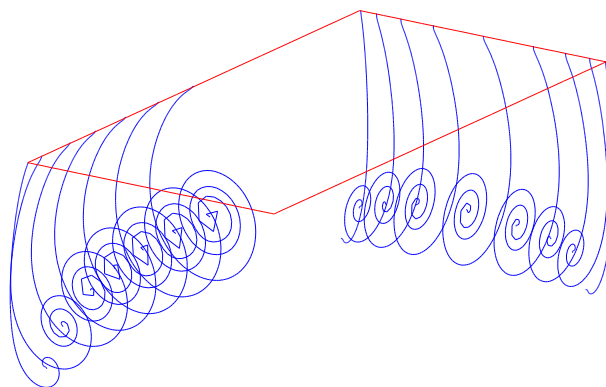
Figure 6: Wake shape for $AR = 2$.
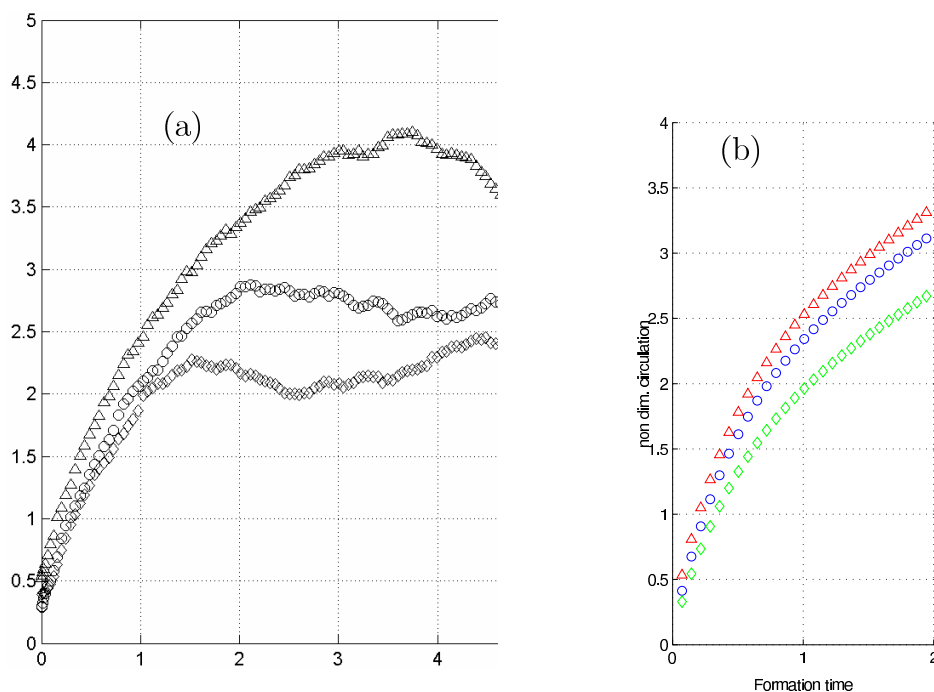
Figure 7: Circulation vs. formation time from (a) Ringuette's experiment and (b) numerical method, for $AR = 2$, triangles - 50% span, circles - 75% span, diamonds - 90% span.

In Fig. 7 we make a comparison between the experiment (plot (a)) and our numerical method (plot (b)). We plot here the total circulation of a chord-wise section in the wake versus the formation time. The formation time is a non-dimensional time defined as $t_{form} = U_0 \cdot t/c$, where c is the chord length. The plots are for three different chord-wise sections: triangles denote the circulation at 50% of span, circles at 75% of span and diamonds at 90% of span. It can be seen

that the plots look very similar until the pinch-off occurs. After that, the circulation from the experiment would not grow as fast anymore and trail after the numerical results. This can be seen even better in Fig. 8.

Plots (a) and (b) show the total circulation at 50% span from experiment and numerical method, respectively. We can see that the plots are identical until about formation time $t_{form} = 3$, i.e., until the plate has traveled three chord lengths. Accordingly, plots (c) and (d) show the circulation at 75% span while (e) and (f) show the circulation at 90% span. On the right is always the experimental result. We can see that for the 75% span case the similarity goes up to $t_{form} = 2$ while in the 90% span case up to $t_{form} = 1.5$. On the left, we also have the shapes of the corresponding sections taken from the experiment at given formation times.

Aspect Ratio 6

For a wing of aspect ratio 6, the effects due to the tip are less significant than in the $AR = 2$ case. It can be seen from Fig. 9 that the vortices near both chord-wise and span-wise center sections have more roll-ups than the ones near the corresponding edges. This is, again, in perfect agreement with what we found in the previous subsection, where it was showed (see Fig. 5) that there is more circulation near the bound center sections than near the edges. This implies that less circulation is shed in the free sheet near the edges, making the vortices weaker. However, in this case this can be seen better along span-wise sections due to the higher aspect ratio plate. Also, from the same plots (see Fig. 5) we expect the vortices to be stronger along the chord wise sections compared to those released along span-wise sections since the corresponding total circulation is bigger. This is obviously more pronounced here than in the $AR = 2$ case.

In both numerical and experimental setup, a plate with chord $c = 5$ and aspect ratio $AR = 6$ is used (for the experiment the measuring unit was centimeter). The plate velocity is $U_0 = 6$, and, for the numerical method, we choose a time step of $dt = 0.003$ and a blob $\delta = 0.2$. Our numerical bound sheet is represented by a 31x31 point mesh.

In Fig. 10 we make a comparison between the experiment (plot (a)) and our numerical method (plot (b)). We plot here again the total circulation of a chord-wise section in the wake versus the formation time. The plots are for three different chord-wise sections: triangles denote the circulation at 50% of span, circles at 75% of span and diamonds at 90% of span. It can be seen that the plots look very similar until the pinch-off occurs. After that, the circulation from the experiment would not grow as fast anymore and trail after the numerical results. This can be seen even better in Fig. 11.

Plots 10(a) and 10(b) show the total circulation at 50% span from experiment and numerical method, respectively. We can see that the plots are in very good agreement all the way up to formation time $t_{form} = 4.5$, i.e., until the plate has traveled four and a half chord lengths. Accordingly, plots 10 (c) and 10(d) show the circulation at 75% span, while 10(e) and 10(f) show the circulation at 90% span. On the right is always the experimental result. We can see that for the 75% case the similarity goes up to $t_{form} = 3$ while in the 90% case up to $t_{form} = 2$. On the left, we also have the shapes of the corresponding sections taken from the experiment at given formation times. The plot of the circulation of the leading edge vortex is also included in some of these plots (x's and/or crosses). One can see that after a while the circulation of this
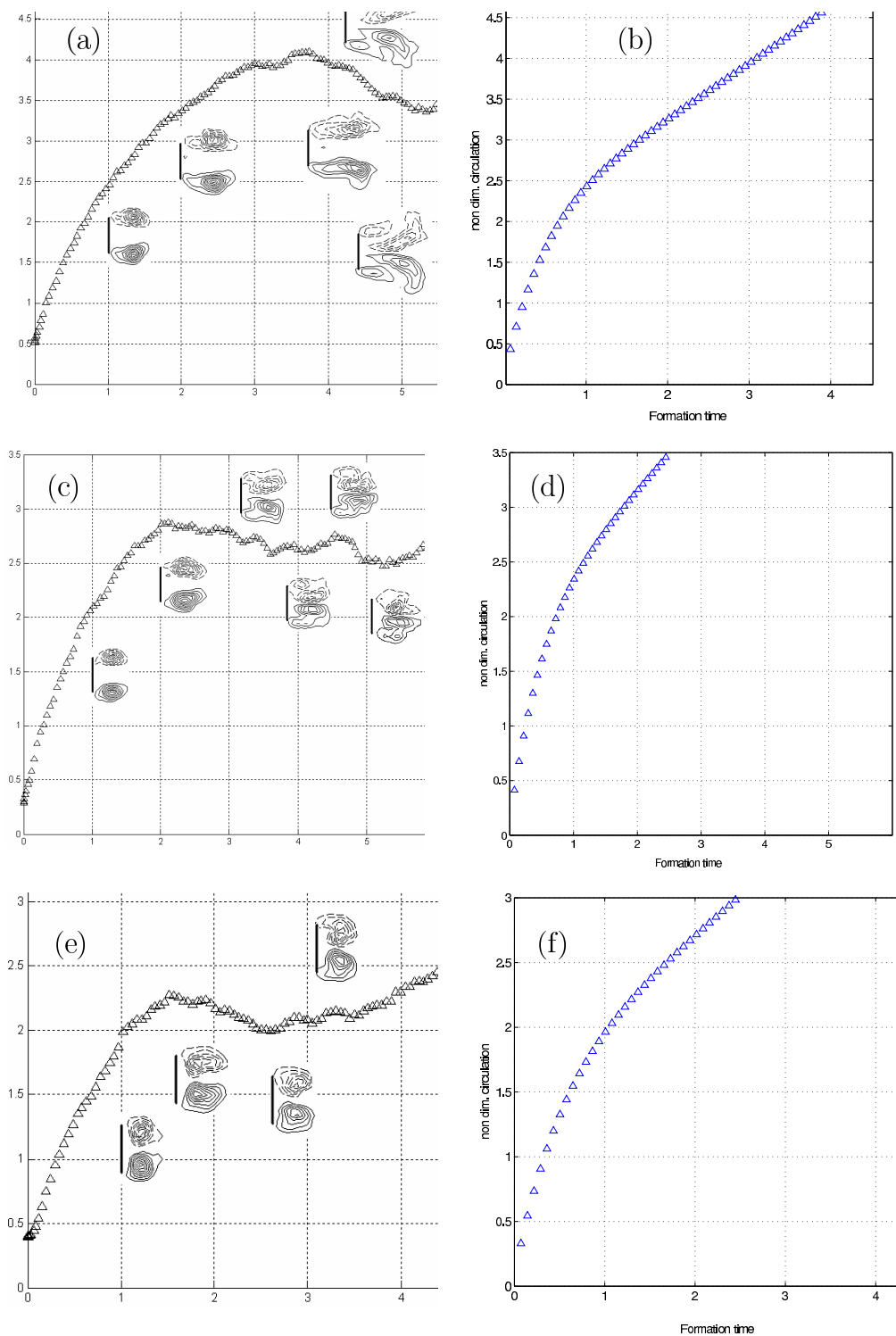
Figure 8: Total circulation versus formation time for $AR = 2$. Left column - Ringuette's experiment results, right column - our numerical results. (a)&(b) 50% span, (c)&(d) 75% span, (e)&(f) 90% span.
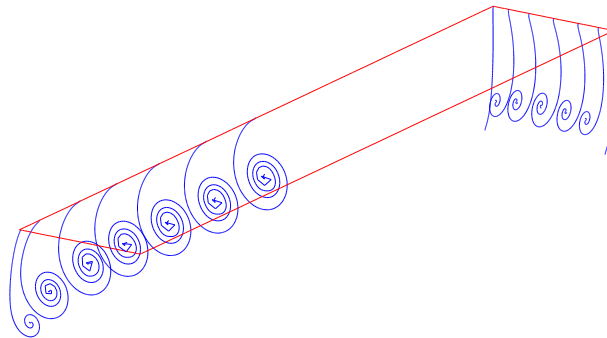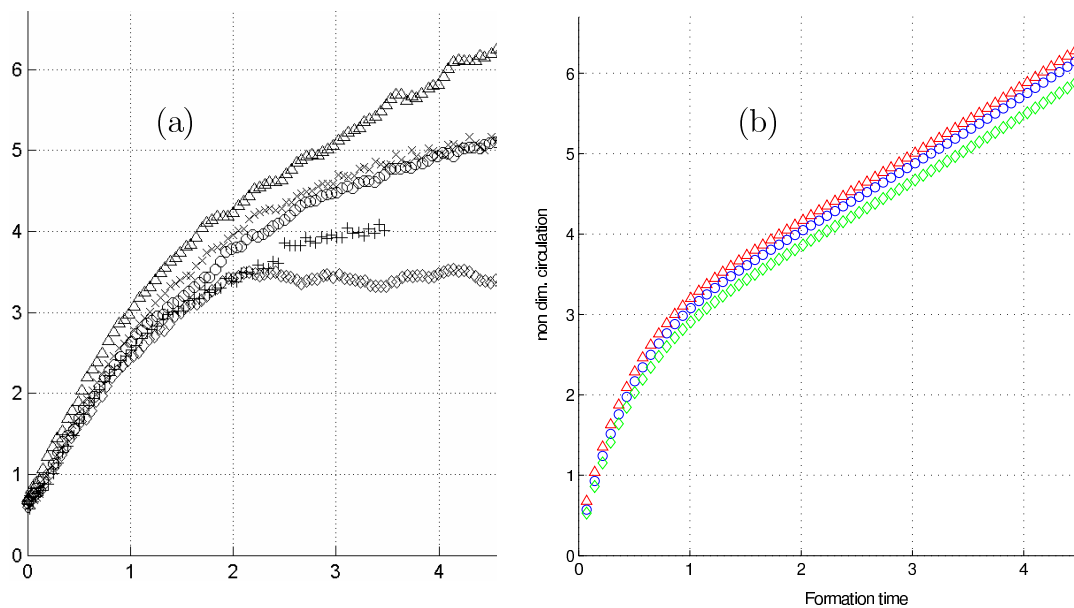
Figure 9: Wake shape for $AR = 6$.

Figure 10: Circulation vs. formation time from (a) Ringuette's experiment and (b) numerical method, for $AR = 6$, triangles - 50% span, circles - 75% span, diamonds - 90% span.

LEV will trail the total circulation, implying separation.

3.5 Numerical results for a three-dimensional square wing

In this subsection, we present our numerical results for a square plate when $AR = 1$. In this case, the finite-wing effects are the strongest. Unfortunately we could not find an experiment to match the square plate model. Based on the previous comparisons for $AR > 1$, we are confident our results are qualitatively correct.

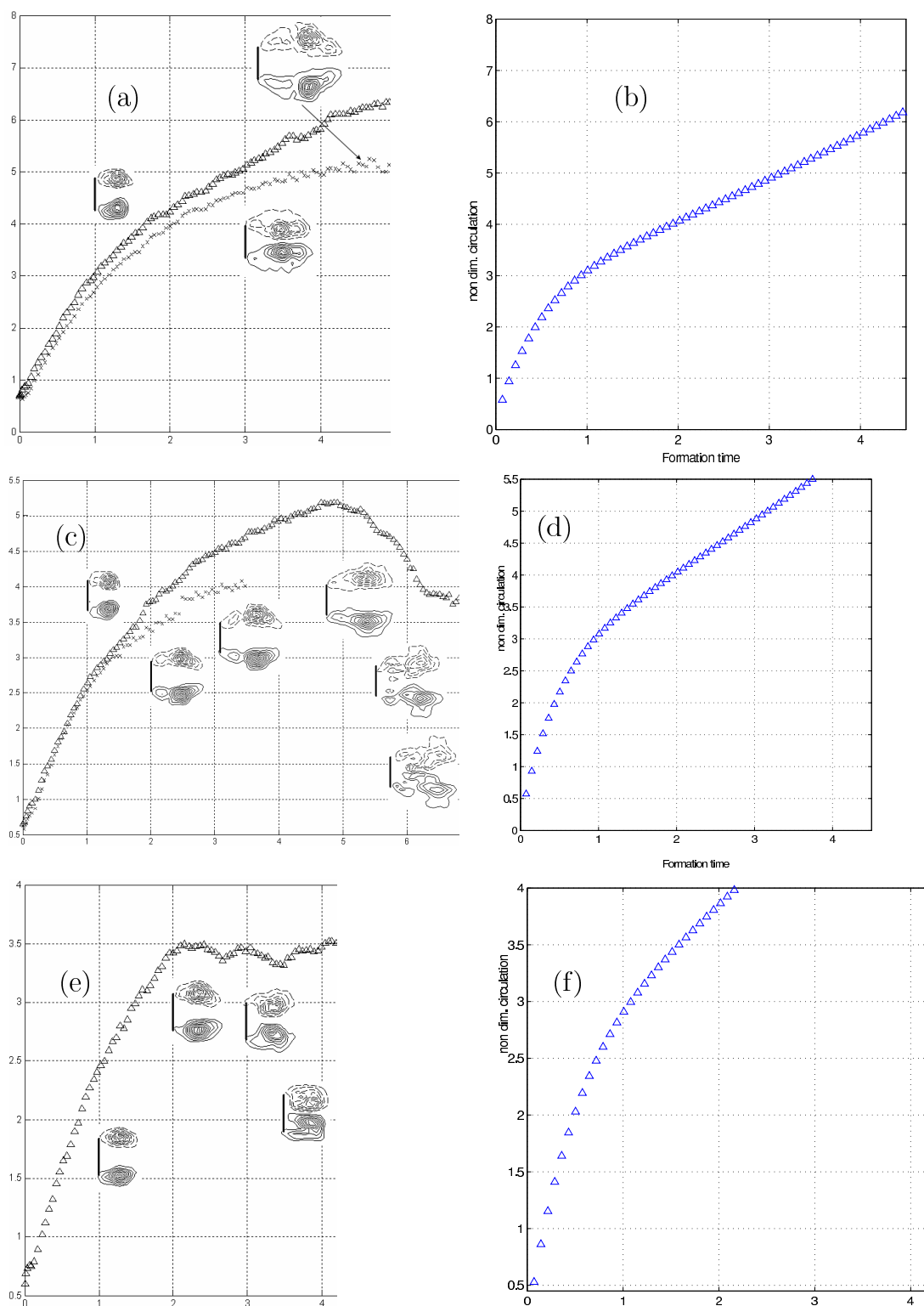For the numerical simulations, we choose a square plate of length 2 represented by a 31x31

Figure 11: Total circulation versus formation time for $AR = 6$. Left column - Ringuette's experiment results, right column - our numerical results. (a)&(b) 50% span, (c)&(d) 75% span, (e)&(f) 90% span.
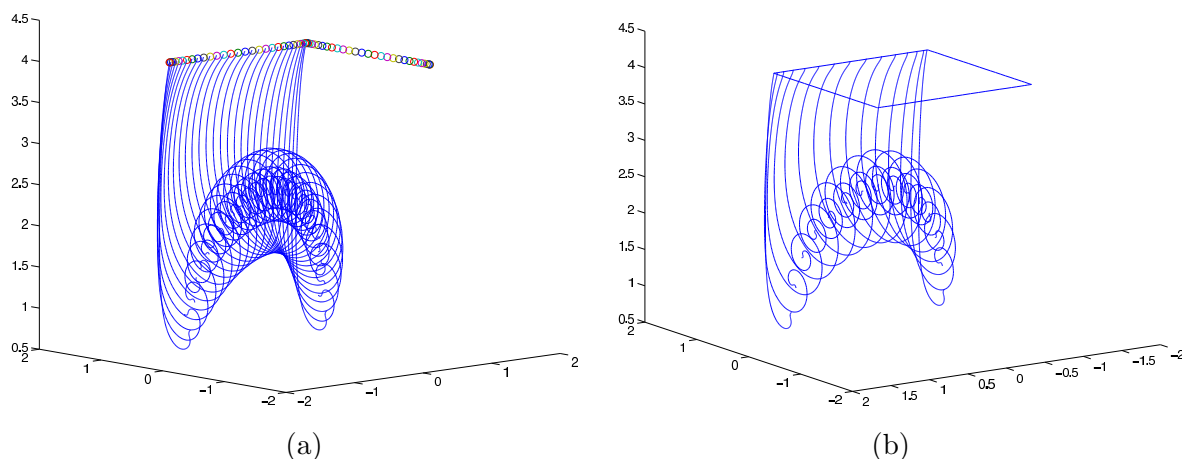
Figure 12: Wake shape in the case of a square plate. (a) has twice as many vortices as (b).
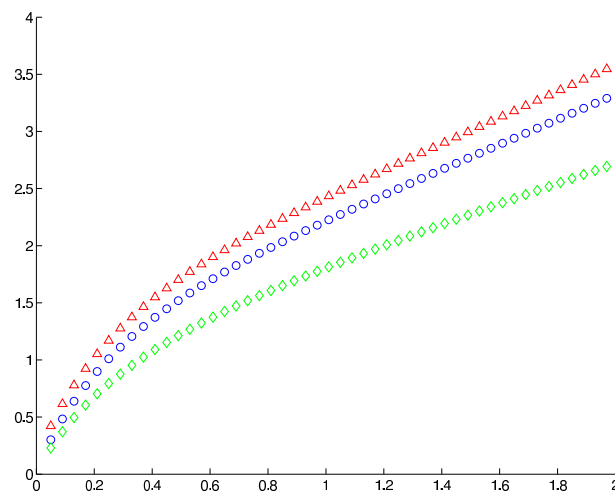

Figure 13: Circulation vs. formation time - numerical results, for $AR = 1$, triangles - 50% span, circles - 75% span, diamonds - 90% span.

point mesh. The plate is moving upward with velocity $U_0 = 1$ and data are collected every $dt = 0.01$ time step. The blob again is chosen to be $\delta = 0.2$, and the code is stopped after 400 time steps. This is equivalent to a formation time of 4.

In Fig. 12(a)&(b), we plot a quarter of the wake since the wake is symmetrical. From this plots we can see very well how the increased circulation shed in the wake near the center sections makes the vortices stronger, with more roll-ups, while the vortices near the edges are weaker with fewer roll-ups. Due to the lack of circulation, the edge vortices are more elongated because the normal velocity is dominant. Plots (a) and (b) are similar, with the only difference that in plot (b) we have half as many vortices as in (a) for a better visualization.

Fig. 13 contains a plot similar to the ones we have already seen in $AR = 2$ and $AR = 6$ cases: total circulation versus formation time. This time though, due to the more powerful finite-wing effects, the separation between the three curves ($\triangle$'s - 50% span, $\circ$'s - 75% span and $\diamond$'s - 90% span) is even more accentuated.

4   Concluding remarks

The main objective of this paper was motivated by our desire to develop an effective three dimensional method for the study of the wake behind a flying wing. The three-dimensional method presented here is just a first step in this direction. The current method shows some very nice behavior compared with the experiment and demonstrates how efficient a direct generalization of the two-dimensional theory could be when some three-dimensional considerations are taken into account. The three-dimensional numerical method we presented here could provide the basis for a further investigation of a possible generalization of Wu's method to three dimensions [22]. The current model still gives relatively poor approximations near the corners of the plate, where the three dimensional effects are the strongest. Also, it cannot capture the helical patterns observed near the corners by Ringuette's experiments. If we can generalize Wu's theory to three space dimensions, we can incorporate this three dimensional theory into our numerical method. Then we can capture the high order nonlinear 3D effects accurately by our numerical method, which will provide an effective model to simulate accurately the motion of a moving surface.

Acknowledgements

References

[1] M. Brady, A. Leonard and D. I. Pullin, Regularized vortex sheet evolution in three dimensions, J. Comput. Phys., 146 (1998), 520–545.

[2] P. A. Chamara and B. D. Coller, Double flutter in an aeroelastic system, Amer. Inst. Aeronaut. Astronaut., 39 (2001), 1206-1208.

[3] A. J. Chorin and P. S. Bernard, Discretization of a vortex sheet, with an example of roll-up, J. Comput. Phys., 13 (1973), 423–429.

[4] W. J. Davenport, M. C. Rife, S. I. Liapis and G. J. Follin, The structure and development of a wing-tip vortex, J. Fluid Mech., 312 (1995), 67–106.

[5] S. Dhawan, Bird Flight, Bangalore, Indian Academy of Sciences, 1991.

[6] M. H. Dickinson, F. O. Lehmann and S. P. Sane, Wing rotation and the aerodynamic basis of insect flight, Science, 284 (1999), 1954–1960.

[7] C. P. Ellington, The aerodynamics of hovering insect flight, Philos. Trans. Roy. Soc. London Ser. B, 305 (1984), 1–181.

[8] T. Y. Hou, V. G. Stredie and T. Y. Wu, Mathematical modeling and simulation of aquatic and aerial animal locomotion in two dimensions, preprint, 2005.

[9] J. Katz and A. Plotkin, Low-speed Aerodynamics, 2nd edition, Cambridge University Press, NY, 2001.

[10] R. Krasny, Vortex Sheet Computations: Roll-up, wakes, separation, Lectures in Appl. Math., 28 (1991), 385–402.

[11] K. Lindsay and R. Krasny, A particle method and adaptive treecode for vortex sheet motion in three-dimensional flow, J. Comput. Phys., 172 (2001), 879–907.

[12] D. W. Moore, The stability of an evolving two-dimensional vortex sheet, Mathematika, 23 (1976), 35–44.

[13] M. Nitsche and R. Krasny, Numerical study of vortex ring formation at the edge of a circular tube, J. Fluid Mech., 276 (1994), 139–161.

[14] D. I. Pullin, The large-scale structure of of unsteady self-similar rolled-up vortex sheets, J. Fluid Mech., 88 (1978), 401–430.

[15] M. J. Ringuette, Vortex Formation and Drag on Low Aspect Ratio, Normal Flat Plates, Ph.D. Thesis, California Institute of Technology, 2004.

[16] N. Rott, Diffraction of a weak shock with vortex generation, J. Fluid. Mech., 28 (1956), 111–128.

[17] P. G. Saffman, Vortex Dynamics, Cambridge University Press, Cambridge, 1992.

[18] T. Theodorsen, General theory of aerodynamic instability and the mechanism of flutter, National Advisory Committee for Aeronautics, Report No. 496, 1935.

[19] Z. J. Wang, J. M. Birch and M. H. Dickinson, Unsteady forces and flows in low Reynolds number hovering flight: Two-dimensional computations vs robotic wing experiments, J. Exp. Biol., 207 (2004), 449–460.

[20] Z. J. Wang, Two dimensional mechanism for insect hovering, Phys. Rev. Lett., 85 (2000), 2216–2219.

[21] T. Y. Wu, Introduction to the scaling of aquatic animal locomotion, in: T. Pedley (Ed.), Scale Effects in Animal Locomotion, Academic Press, New York and London, 1977, pp. 203–232.

[22] T. Y. Wu, On theoretical modeling of aquatic and aerial animal locomotion, Adv. Appl. Mech., 38 (2001), 291–352.